

IDENTIFICATIONS OF FOUR *INTEGRAL* SOURCES IN THE GALACTIC PLANE VIA *CHANDRA* LOCALIZATIONS

JOHN A. TOMSICK¹, SYLVAIN CHATY², JEROME RODRIGUEZ², LUIGI FOSCHINI³, ROLAND WALTER⁴, PHILIP KAARET⁵

Accepted by the Astrophysical Journal

ABSTRACT

Hard X-ray imaging of the Galactic plane by the *INTEGRAL* satellite is uncovering large numbers of 20–100 keV “IGR” sources. We present results from *Chandra*, *INTEGRAL*, optical, and IR observations of 4 IGR sources: 3 sources in the Norma region of the Galaxy (IGR J16195–4945, IGR J16207–5129, and IGR J16167–4957) and one that is closer to the Galactic center (IGR J17195–4100). In all 4 cases, one relatively bright *Chandra* source is seen in the *INTEGRAL* error circle, and these are likely to be the soft X-ray counterparts of the IGR sources. They have hard 0.3–10 keV spectra with power-law photon indices of $\Gamma = 0.5$ –1.1. While many previously studied IGR sources show high column densities ($N_{\text{H}} \sim 10^{23-24} \text{ cm}^{-2}$), only IGR J16195–4945 has a column density that could be as high as 10^{23} cm^{-2} . Using optical and IR sky survey catalogs and our own photometry, we have obtained identifications for all 4 sources. The *J*-band magnitudes are in the range 14.9–10.4, and we have used the optical/IR spectral energy distributions (SEDs) to constrain the nature of the sources. Blackbody components with temperature lower limits of $>9400 \text{ K}$ for IGR J16195–4945 and $>18,000 \text{ K}$ for IGR J16207–5129 indicate that these are very likely High-Mass X-ray Binaries (HMXBs). However, for IGR J16167–4957 and IGR J17195–4100, low extinction and the SEDs indicate later spectral types for the putative companions, indicating that these are not HMXBs.

Subject headings: stars: neutron — X-rays: stars — infrared: stars — stars: individual (IGR J16195–4945, IGR J16207–5129, IGR J16167–4957, IGR J17195–4100)

1. INTRODUCTION

The hard X-ray imaging of the Galactic Plane by the *International Gamma-Ray Astrophysics Laboratory* (*INTEGRAL*, Winkler et al. 2003) is uncovering a large number of new or previously poorly studied high energy sources. During the first two years of *INTEGRAL* operations (2002 October – 2004 September), 56 new “IGR” sources were discovered (Bird et al. 2006), and many more IGR sources have been discovered to date. *INTEGRAL* is also detecting many sources that are present in other X-ray catalogs but were not targets of focused studies until they were shown to be strong emitters of hard X-rays by *INTEGRAL*. If these sources are included, well over 100 IGR sources have been found⁶. All or nearly all of the IGR sources have been found in the 20–50 keV band with the Imager on Board the *INTEGRAL* Satellite (IBIS) coded aperture mask instrument (Ubertini et al. 2003; Lebrun et al. 2003). Large numbers of IGR sources have been found because of the combination of hard X-ray imaging with 12' angular resolution, a large field of view (9° by 9° fully coded FOV for IBIS), and the *INTEGRAL* observing plan, which emphasizes observations of the Galactic Plane.

Follow-up observations of the IGR sources have shown a diversity of source types, including Low-Mass X-ray Binaries (LMXBs), High-Mass X-ray Binaries (HMXBs), Active Galactic Nuclei, Cataclysmic Variables as well as other source

types. While some of the sources have proved to be transient, others have been consistently detected in X-rays in multiple *INTEGRAL* observations as well as by other current and previous X-ray instruments, suggesting that they are persistent. One sub-group of IGR sources exhibits persistent but highly variable X-ray emission. These sources lie within a few degrees of the Galactic Plane and show some evidence for clustering near Galactic spiral arms (Lutovinov et al. 2005a). Their X-ray fluxes are typically ~ 1 –10 millicrab in the hard X-ray band (Dean et al. 2005), and their luminosities are mostly unknown due to large uncertainties on their distances, but they may have luminosities of $10^{33-36} \text{ ergs s}^{-1}$ if they are at typical 1–10 kpc Galactic distances.

Although X-ray, optical, and infrared (IR) observations of this group of persistent, Galactic IGR sources show that they do not have uniform properties, some trends have been identified. For many of these sources, their X-ray spectra show high column densities with values of N_{H} well in excess of the levels expected due to interstellar material. The most extreme example is IGR J16318–4848, for which $N_{\text{H}} \sim 2 \times 10^{24} \text{ cm}^{-2}$ (Matt & Guainazzi 2003; Walter et al. 2003), and there are also several other sources with values of N_{H} in the $10^{23-24} \text{ cm}^{-2}$ range (e.g., Rodriguez et al. 2003; Combi et al. 2004; Beckmann et al. 2005). Many of the Galactic IGR sources also exhibit X-ray pulsations, indicating the presence of a neutron star. Pulsations are detected for at least 5 of the persistent IGR sources with periods of 139–1303 s (e.g., Lutovinov et al. 2005b; Bodaghee et al. 2006). Finally, in some cases for which optical or IR spectra of IGR sources have been obtained, high-mass stellar companions have been found. IGR J16318–4848 harbors an unusual supergiant B[e] star, and the IR spectra also show P Cygni profiles, suggesting the presence of a strong stellar outflow (Filliatre & Chaty 2004). Another example is IGR J17391–3021 (= XTE J1739–302), which also contains a supergiant (Smith et al. 2006; Noguera et al. 2006).

Here, we present results for X-ray, optical, and IR follow-

¹ Center for Astrophysics and Space Sciences, Code 0424, University of California at San Diego, La Jolla, CA, 92093, USA (e-mail: jtomsick@ucsd.edu)

² AIM - Astrophysique Interactions Multi-échelles (UMR 7158 CEA/CNRS/Université Paris 7 Denis Diderot), CEA Saclay, DSM/DAPNIA/Service d'Astrophysique, Bât. 709, L'Orme des Merisiers, FR-91 191 Gif-sur-Yvette Cedex, France

³ INAF/IASF - Bologna, Via Gobetti 101, 40129 Bologna, Italy

⁴ ISDC, Chemin d'Ecogia, 16, 1290 Versoix, Switzerland

⁵ Department of Physics and Astronomy, University of Iowa, Iowa City, IA 52242, USA

⁶ A current list of IGR sources is available at <http://isdc.unige.ch/~rodrigue/html/igrsources.html>

up studies of 4 IGR sources that are in the Galactic Plane. Three of the sources (IGR J16195–4945, IGR J16207–5129, IGR J16167–4957) are in the Norma region of the Galaxy (i.e., close to the tangent to the Norma spiral arm) at $332^\circ < l < 334^\circ$, and the fourth (IGR J17195–4100) is about half-way between the Norma region and the Galactic center at $l = 347^\circ$. Although none of the sources have been previously well-studied, it has been pointed out that IGR J16195–4945 is probably the *Advanced Satellite for Cosmology and Astrophysics* (ASCA) source AX J161929–4945 (Sugizaki et al. 2001; Sidoli et al. 2005). The 2–10 keV ASCA spectrum of this source is well-described by a very hard power-law with a photon index of $\Gamma = 0.6_{-0.5}^{+0.8}$ and a relatively high column density of $N_{\text{H}} = (12_{-4}^{+8}) \times 10^{22} \text{ cm}^{-2}$. Based on its X-ray properties, it has been suggested that the source is a neutron star HMXB (Sidoli et al. 2005; Bird et al. 2006). IGR J16167–4957 and IGR J17195–4100 have been tentatively identified with *ROSAT* sources (Stephen et al. 2005), but it appears that *INTEGRAL* is the first X-ray satellite to detect IGR J16207–5129. The nature of these 3 sources is completely uncertain (Bird et al. 2006).

In this work, we use observations with the *Chandra X-ray Observatory* (Weisskopf et al. 2002) to obtain sub-arcsecond X-ray positions for the 4 sources (§2) and to determine whether the sources are associated with known sources (§3). In §4 and §5, we present a study of the *Chandra* and *INTEGRAL* spectra. In §6, we report on optical and IR photometry of these sources we made at ESO’s New Technology Telescope (NTT), and we combine these measurements with those available in optical and IR catalogs in order to constrain the optical and IR spectral energy distributions (§7). In §8 and §9, we discuss our results and present our conclusions.

2. CHANDRA OBSERVATIONS AND SOURCE DETECTION

We obtained short, ~ 5 ks, *Chandra* observations of the fields of IGR J16195–4945, IGR J16207–5129, IGR J16167–4957, and IGR J17195–4100 with the primary goal of localizing the sources to facilitate IR and optical identifications. We chose targets located close to the Galactic Plane that were detected in the 20–40 keV band during our 2003 February *INTEGRAL* observation of the black hole transient 4U 1630–47 (Tomsick et al. 2004, 2005) and that were also reported in the first and second catalogs of *INTEGRAL* sources (Bird et al. 2004, 2006). Consistent hard X-ray detections gave us reason to believe that these were persistent sources and that the probability of detection with *Chandra* was high.

Table 1 shows the Observation IDs (ObsIDs) and times of our *Chandra* observations of the 4 IGR sources, which took place between 2005 April and July. We used the Advanced CCD Imaging Spectrometer (ACIS, Garmire et al. 2003) with the center of the $3'$ *INTEGRAL* error circle placed at the nominal aimpoint for the ACIS-I array. Although the effective exposure times are lower in the gaps between ACIS-I chips, we used a dithering pattern with an amplitude twice as large as the standard pattern to achieve a more uniform sensitivity over the *INTEGRAL* error circle. In processing the data, we started with the “level 1” event list produced by the standard data processing with ASCDS versions between 7.5.3 and 7.6.2. For further processing, we used the *Chandra* Interactive Analysis of Observations (CIAO) version 3.3.0.1 software and Calibration Data Base (CALDB) version 3.2.1. We used the CIAO routine `acis_process_events` to obtain a “level 2” event list and image.

The *Chandra* images are shown in Figure 1. For each target,

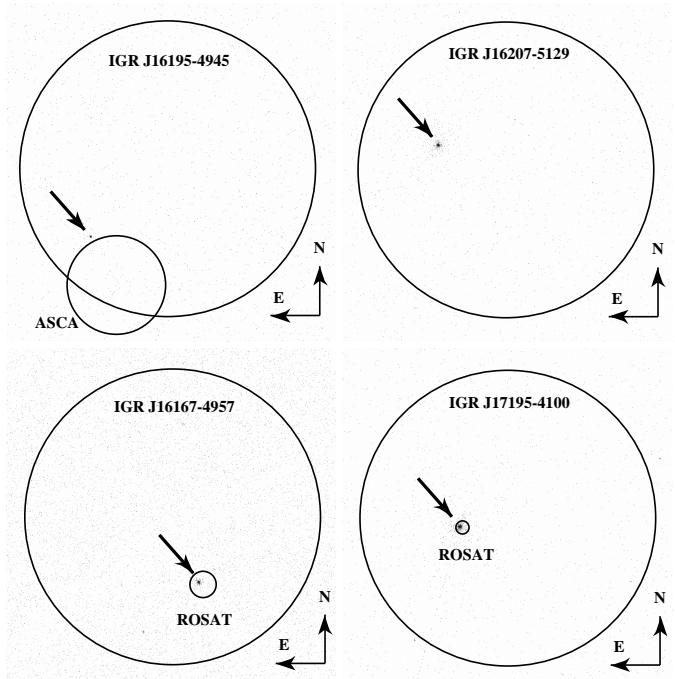


FIG. 1.— *Chandra* 0.3–10 keV images of the 4 IGR sources. The large circles are the $3'$ *INTEGRAL* error circles. In three cases, ASCA or *ROSAT* counterparts have been suggested, and their error circles are also shown. Arrows point to the brightest *Chandra* source detected in each observation, and these are very likely the soft X-ray counterparts to the IGR sources. The lengths of the N and E arrows are $1'$.

we searched for sources in a 7×7 arcmin² region that includes the full *INTEGRAL* error circle. We restricted the energy range to 0.3–10 keV and used the CIAO routine `wavdetect` (Freeman et al. 2002). Based on the image size of 854-by-854 pixels and our detection threshold of 10^{-6} (see Freeman et al. 2002, for a precise definition), we would expect to detect $\lesssim 1$ spurious source. For ObsIDs 5471, 5472, 5473, and 5474, we detected 4, 7, 4, and 7 sources, respectively. The brightest sources for these four ObsIDs have 183, 678, 866, and 676 counts, respectively, while the remaining sources have between 3 and 24 counts. In addition, each of these four brightest sources are located within the respective *INTEGRAL* error circles (see Figure 1), making it very likely that these sources are, in fact, the soft X-ray counterparts of the IGR sources. In the following, we focus on the properties of these four sources and primarily refer to them by their IGR names (even though *Chandra* names are also given to the sources).

3. CHANDRA POSITIONS AND ASSOCIATIONS WITH KNOWN SOURCES

Table 2 provides the *Chandra* positions for the four sources. The positions come from the `wavdetect` analysis described above, and the position uncertainties are $0''.6$. This value is the nominal *Chandra* pointing accuracy, and the statistical errors calculated by `wavdetect` are negligible in comparison. Here, we use the SIMBAD database to determine if the *Chandra* sources are associated with previously known sources.

For IGR J16195–4945, the *Chandra* source CXOU J161932.2–494430 lies $1'.1$ from the best ASCA position for AX J161929–4945, which is just outside the $1'$ ASCA error circle (see Figure 1). While Sugizaki et al. (2001) quote ASCA position uncertainties of $1'$, a careful analysis by

Ueda et al. (1999) shows that the 90% confidence error radii for *ASCA* sources are in the range $0'.6$ – $0'.8$, depending on the detection significance. Thus, the $1'$ error circle can be considered to be slightly larger than a 90% confidence error circle. Still, CXOU J161932.2–494430 and AX J161929–4945 are close enough to consider the association likely. An association between IGR J16195–4945, AX J161929–4945, and the B1/B2 Ia supergiant HD 146628 has also been suggested (Sidoli et al. 2005; Tomsick et al. 2004; Sugizaki et al. 2001). However, the *Chandra* position is $1'.2$ away from HD 146628, clearly ruling out this association. There are no sources in the SIMBAD database within $1'$ of the *Chandra* position.

There is no evidence that IGR J16207–5129 was previously detected in the X-ray band. While the source is bright enough to be seen in the *ASCA* Galactic Plane Scans, it lies just outside of the region that was observed at a Galactic latitude of $b = -1.05^\circ$. A possible association between IGR J16207–5129 and the A1 IVe star HD 146803 was suggested (Tomsick et al. 2004; Masetti et al. 2006b); however, this is ruled out by the fact that the positions for HD 146803 and CXOU J162046.2–513006 are not compatible. There are no sources in the SIMBAD database within $1'$ of the *Chandra* position.

For IGR J16167–4957 and IGR J17195–4100, the *Chandra* positions confirm associations with 1RXS J161637.2–495847 and 1RXS J171935.6–410054, respectively (see Figure 1). A SIMBAD search at the *Chandra* position of CXOU J161637.7–495844 reveals only IGR J16167–4957 and the *ROSAT* source within $1'$. For IGR J17195–4100, the only other SIMBAD source within $1'$ of CXOU J171935.8–410053 is USNO-B1.0 0489–0511283. This USNO source is $0''.70$ from the *Chandra* position and must be considered as a possible optical counterpart. We investigate this possibility further in §6.

4. CHANDRA ENERGY SPECTRA AND LIGHT CURVES

We produced 0.3–10 keV energy spectra for each of the four bright *Chandra* sources using the CIAO tool `dmextract` to produce the spectrum and the tools `mkacisrmf` and `mkarf` to produce the files needed to characterizing the instrument response. We used a circular source extraction region with a radius of $2''.5$ and an annular background region centered on the source with inner and outer radii of $10''$ and $60''$, respectively. Given that two of the sources are close to the gaps between the ACIS chips, we produced exposure maps to determine the effective exposure time for each source. The sources IGR J16207–5129 and IGR J17195–4100 (ObsIDs 5472 and 5474) received the full exposure time, but IGR J16195–4945 (ObsID 5471) and IGR J16167–4957 (ObsID 5473) received 70% and 67% of the full exposure time, respectively. The CIAO tool `mkarf` automatically accounts for the reduced instrument response near chip boundaries.

We fitted the spectra using the software package XSPEC 11.3.2o. Originally, we rebinned the spectra and fitted them using χ^2 -minimization. After rebinning, the spectrum for the lowest count rate source (IGR J16195–4945) had 9 bins with an average of 20 counts per bin, while we used 12-bin spectra for the other 3 sources. We fitted the spectra using a model consisting of an absorbed power-law, and, based on the results for other IGR sources, it would not be surprising if the column density has intrinsic and interstellar contributions (e.g., Walter et al. 2003; Revnivtsev 2003). The absorbed power-law fit is acceptable ($\chi^2/\nu = 4.0/6$) for IGR J16195–4945, but we obtained very poor fits for the other three sources with val-

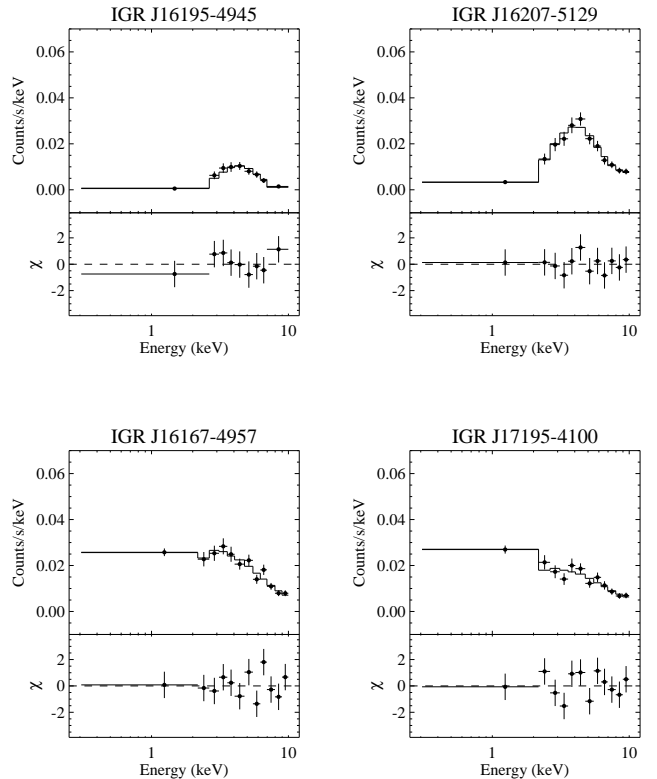


FIG. 2.— *Chandra* energy spectra and residuals for the four IGR sources fitted with an absorbed power-law model. For IGR J16207–5129, IGR J16167–4957, and IGR J17195–4100, a pile-up correction is included in the model.

ues of χ^2 between 46 and 83 for 9 degrees of freedom (dof). Large positive residuals above ~ 6 keV are the main reason for the poor fits. This suggests that photon pile-up (Davis 2001) is affecting these three spectra, and, indeed, one expects pile-up to significantly impact the spectral shape for sources with count rates as high as we observe for the three brighter sources (0.13 – 0.18 s $^{-1}$). We refitted the three affected spectra after including the XSPEC `pileup` model (Davis 2001), and the quality of the fits improves enormously with χ^2 values of 3.7, 8.7, and 9.2 (8 dof) for IGR J16207–5129, IGR J16167–4957, and IGR J17195–4100, respectively. Comptonization models (e.g., `comptt` in XSPEC) approximate a power-law shape in the 0.3–10 keV band and provide fits of similar quality to the power-law fits. While a thermal blackbody model can adequately describe the spectrum of the fainter source, such a model provides very poor fits to the spectra of the three brighter sources. Even if the pile-up correction is included, an absorbed blackbody model gives χ^2 values between 32 and 98 for 8 dof. We conclude that these three spectra are non-thermal, and we focus on the power-law model below.

Another signature of photon pile-up is the flattening of the point spread function (PSF), and this causes the three brighter sources to appear extended when their radial profiles (i.e., surface brightness vs. angle from the source position) are compared to the profiles of point sources that are unaffected by pile-up. We studied the radial profiles of the 4 IGR sources as a check of the pile-up correction, and we conclude that the PSF distortions are well-explained by pile-up only and that the pile-up corrections we apply in performing the spectral

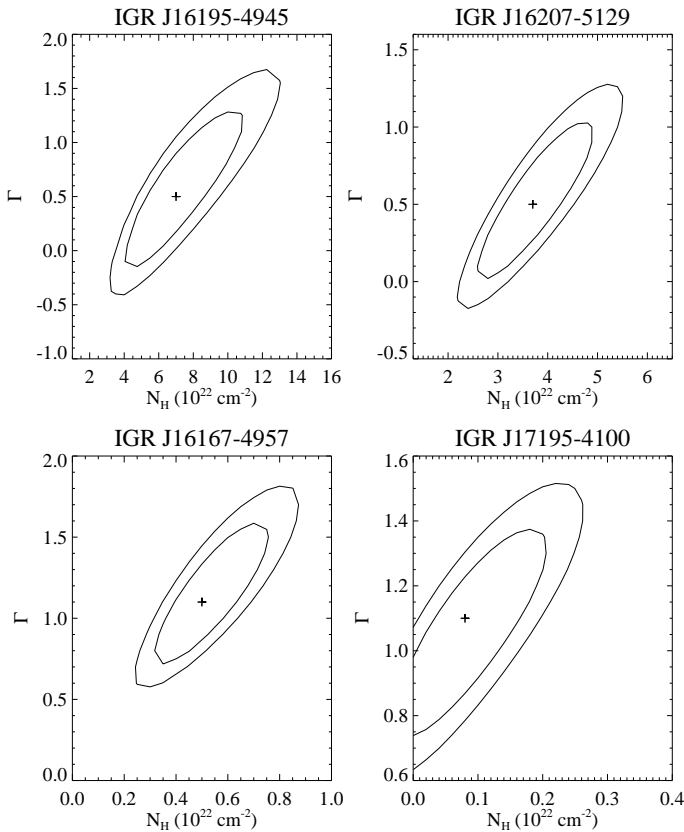


FIG. 3.— Error contours for the parameters N_{H} and Γ from the fits to the *Chandra* spectra. The inner contour is 68% confidence ($\Delta C = 2.3$) and the outer contour is 90% confidence ($\Delta C = 4.6$).

fits are correct.

Figure 2 shows the 0.3–10 keV spectra and residuals for the absorbed power-law fits (with the pile-up correction), and Table 3 provides the values of the spectral parameters. To obtain these values, we refitted the spectra by minimizing the Cash “C”-statistic (Cash 1979), which is an improvement over χ^2 -minimization for spectra with small numbers of counts as the Cash analysis does not require discarding information by rebinning the spectra. While none of the sources show the extremely high column densities that have been seen for some of the IGR sources, the measured values of N_{H} for IGR J16195–4945 and IGR J16207–5129 are $7^{+5}_{-3} \times 10^{22}$ and $3.7^{+1.4}_{-1.2} \times 10^{22}$ cm^{-2} (90% confidence errors), placing them somewhat above their respective Galactic column densities of 2.2×10^{22} and 1.7×10^{22} cm^{-2} (Dickey & Lockman 1990). IGR J16167–4957 and IGR J17195–4100 have values of N_{H} that are significantly lower than their Galactic column densities.

All the sources are intrinsically hard in the 0.3–10 keV band based on the measured values of the power-law photon index. As shown in Table 3, the best fit values of Γ range from 0.5 to 1.1, and, in all cases, the spectra are constrained so that $\Gamma < 1.6$ based on the 90% confidence ($\Delta C = 2.7$) error bars. While the errors on the individual parameters indicate very hard spectra, we also calculated error contours to account for possible correlations between N_{H} and Γ . The contour plots in Figure 3 show the 68% ($\Delta C = 2.3$) and 90% ($\Delta C = 4.6$) confidence error contours, and it is clear that these parameters are significantly correlated for all 4 spectra. While this analysis shows that the error regions are somewhat larger than

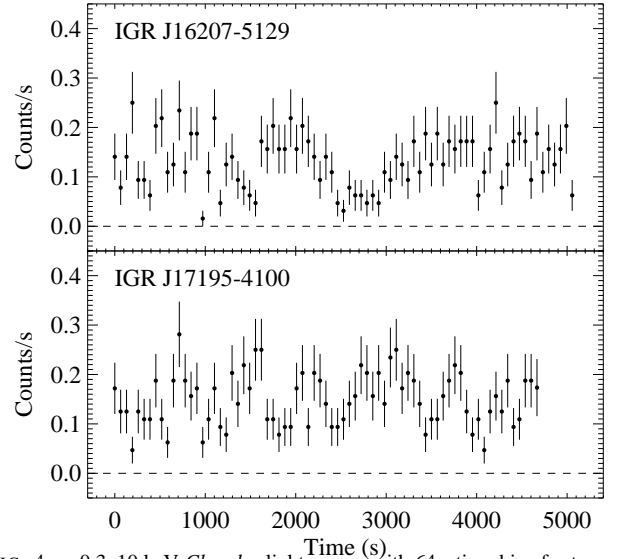


FIG. 4.— 0.3–10 keV *Chandra* light curves with 64 s time bins for two of the IGR sources. IGR J16207–5129 is clearly variable, and there is evidence that IGR J17195–4100 is also variable (see text). The light curves for the other two IGR sources are significantly affected by dithering over the gap between ACIS chips and are not shown.

indicated by the individual parameter values given in Table 3, the spectra are still constrained to be quite hard, with $\Gamma < 1.8$ (90% confidence), and it is still the case that IGR J16195–4945 and IGR J16207–5129 have column densities that are higher than the Galactic values while N_{H} is significantly less than the Galactic values for the other two sources.

We produced 0.3–10 keV light curves with 64 s time bins for all 4 sources. The light curves for IGR J16195–4945 and IGR J16167–4957 are strongly affected by the dithering over gaps between the ACIS chips. In both cases, the count rates drop to zero several times during the observation. In all, about 30% of the time bins are affected, and we do not study the light curves for these 2 sources further. On the other hand, there are no problems with the light curves for IGR J16207–5129 and IGR J17195–4100, and these are shown in Figure 4. The clearest variability is seen for IGR J16207–5129. In the middle of the observation, the count rate drops to about a third of its average level, remains there for ~ 500 s, and then recovers. We formally tested for variability by fitting each light curve with a constant and obtained $\chi^2/\nu = 163/78$ and $\chi^2/\nu = 100/72$ for IGR J16207–5129 and IGR J17195–4100, respectively. Thus, it is likely that both sources exhibit some variability.

5. INTEGRAL ENERGY SPECTRA

We also produced >22 keV spectra from the IBIS/ISGRI instrument on *INTEGRAL*. The observations used to produce the spectra include all public data available from *INTEGRAL* revolutions 46 to 235 (2003 February 27 to 2004 September 15). We made sky images and mosaics with the Off-line-Analysis Software version 5.1 in 10 energy bands between 22 keV and 250 keV, and we derived average source spectra from the mosaic images. After making vignetting, off-axis, and dead-time corrections, the effective exposure time is 495 ks for IGR J17195–4100 and ~ 165 ks per source for the other 3 sources (see Table 4). Despite the relatively long exposure times, these sources are rather faint for *INTEGRAL*

with 20–50 keV ISGRI count rates between 0.18 ± 0.03 and $0.35 \pm 0.03 \text{ s}^{-1}$ (compared to, e.g., a 20–60 keV count rate of 160 s^{-1} for the Crab Pulsar and Nebula). Thus, the spectra of the IGR sources consist of a relatively small number of energy bins. For IGR J16195–4945, IGR J16207–5129, and IGR J17195–4100, we are able to obtain 4 energy bins in which the source is detected at a significance of at least $4\text{-}\sigma$, and, for IGR J16167–4957, the source is only detected in 2 energy bins.

We fitted the ISGRI spectra with a power-law model, and the results of these fits are given in Table 4. For IGR J16195–4945, IGR J16207–5129, and IGR J17195–4100, acceptable fits are obtained with the power-law model with values of Γ equal to 1.7 ± 0.8 , 1.9 ± 0.5 , and 2.8 ± 0.8 , respectively. While, for IGR J16195–4945, the 90% confidence error region for Γ overlaps with the error region determined using the *Chandra* spectrum, the spectra for IGR J16207–5129 and IGR J17195–4100 are significantly steeper in the 20–50 keV band than in the 0.3–10 keV *Chandra* band. Although the spectrum for IGR J16167–4947 only has 2 energy bins, it is still possible to calculate the value for Γ , and we obtain $4.3^{+1.6}_{-1.4}$, which is significantly steeper than the *Chandra* measurement.

The fact that the spectra are steeper in the ISGRI 20–50 keV band when compared to the *Chandra* 0.3–10 keV band suggests that there is a high energy cut off. To investigate the cut off and to compare the flux levels measured by the two instruments, we performed combined fits for the *Chandra* plus ISGRI spectra. As there is evidence that these sources are variable, and the *Chandra* and ISGRI spectra were not taken simultaneously, it is essential to leave the overall normalization between the two instruments as a free parameter. Leaving all parameters free, we fitted the spectrum for each source with and without an exponential cut off (`highcut` in XSPEC). The cut off is detected at the highest level of significance for IGR J16207–5129 with an improvement in the fit from $\chi^2/\nu = 19.6/11$ to $5.3/9$, corresponding to an F-test significance of 99.7%. The cut off is also marginally statistically significant for IGR J16167–4957, with a 98.4% chance that the cut off is required. The spectra for IGR J16195–4945 and IGR J17195–4100 allow for the possibility that there is a cut off in the ISGRI energy range, but the cut off is not required.

While we allowed the N_{H} , the power-law parameters, α in the pile-up model (for the three brighter sources), the cut off parameters (E_{cut} and E_{fold}), and the overall normalization between the two instruments to be free for the fits described in the previous paragraph, with so many free parameters, the parameter values are very poorly constrained. Thus, we fixed the N_{H} , power-law, and pile-up parameters to the values measured by *Chandra*, and left just the normalization between instruments and the exponential folding energy (E_{fold}) as free parameters in the fit. We fixed the energy at which the exponential cut off begins (E_{cut}) to 10 keV, just above the *Chandra* bandpass. However, it should be noted that, while the *Chandra* spectra do not show any evidence for a spectral cut off, the quality of the spectra and the distortion of the spectra due to pile-up do not allow us to rule out the possibility that the cut off starts at a lower energy. For IGR J16195–4945, IGR J16207–5129, IGR J16167–4957, and IGR J17195–4100, respectively, we obtained ISGRI relative normalizations of $1.1^{+0.9}_{-0.6}$, $0.23^{+0.10}_{-0.08}$, $1.4^{+2.5}_{-0.9}$, and $0.9^{+0.7}_{-0.4}$ as well as the following values for E_{fold} : 32^{+110}_{-14} , 23^{+13}_{-6} , 9^{+7}_{-3} , and 20^{+18}_{-7} keV (90% confidence errors). These values indicate that IGR J16207–5129 was relatively bright during the

Chandra observation compared to the brightness detected by ISGRI in 2003–2004, while the other sources were consistent with a relative normalization of 1.0. Also, it is notable that the range of values we measure for E_{fold} , 9–32 keV, are similar to the values that have been measured for HMXB pulsars (Coburn et al. 2002).

6. IR AND OPTICAL IDENTIFICATIONS

With the $0''.6$ *Chandra* positions for the 4 IGR sources, we are able to search for counterparts to these sources at other wavelengths. We searched the following catalogs: United States Naval Observatory (USNO-B1.0 and USNO-A2.0); Deep Near Infrared Survey of the Southern Sky (DENIS); 2 Micron All-Sky Survey (2MASS); and *Spitzer*'s Galactic Legacy Infrared Mid-Plane Survey Extraordinaire (GLIMPSE). We also performed optical and IR photometry at ESO's New Technology Telescope, and the NTT observations and results are described below.

The USNO catalogs are from optical surveys that cover most of the sky. For the USNO-B1.0, the position accuracies are $0''.2$ and the photometry is good to ± 0.3 magnitudes in *B*, *R*, and *I*. USNO-A2.0 provides $0''.25$ positions and *B* and *R* measurements that are generally accurate to ± 0.5 magnitudes but may be somewhat worse than this in the southern hemisphere. DENIS⁷ is an optical and IR survey, concentrating on the southern hemisphere. The position accuracies are $1''$, and accurate photometry is available in the *I*, *J*, and *K_s* bands. 2MASS⁸ is an all-sky IR survey. The catalog provides very good positions ($0''.2$ accuracy) and accurate photometry in the *J*, *H*, and *K_s* bands. GLIMPSE uses the Infrared Array Camera (IRAC) on *Spitzer* to obtain short exposures of the Galactic plane, covering the Galactic longitude range between 10° and 65° on both sides of the Galactic center and Galactic latitudes within 1° of the plane. Images are obtained in four bands centered at wavelengths of 3.6, 4.5, 5.8, and 8.0 μm . The GLIMPSE team has compiled an on-line catalog⁹ with lists of detected sources, including fluxes and positions accurate to $0''.3$.

On 2004 July 10 between UT 0 and 1 hr, we obtained optical photometry in *B*, *V*, *R*, and *I* bands of the fields of IGR J16195–4945 and IGR J16207–5129 with the spectro-imager EMMI installed on the NTT. We used the large field imaging of EMMI's detector, giving, after 2×2 rebinning, a pixel size of $0''.333$ and a field of view of $9'.9 \times 9'.0$. We used an integration time of 1 s per exposure. We observed 5 photometric standard stars from the optical standard star catalog of Landolt (1992): PG 1633+099, PG 1633+099A, PG 1633+099B, PG 1633+099C, and PG 1633+099D. We also obtained IR photometry in *J*, *H*, and *K_s* bands of IGR J16207–5129 (on 2004 July 8 at UT 4.67 hr), of IGR J16167–4957 (on July 11 at UT 5.67 hr), and of IGR J17195–4100 (on July 11 at UT 6.83 hr) with the spectro-imager SofI installed on the NTT. We used the large field imaging of SofI's detector, giving a pixel size of $0''.288$ and a field of view of $4'.94 \times 4'.94$. These photometric observations were obtained by repeating a set of images for each filter with 9 different $30''$ offset positions, including the targets, with an integration time of 60 s for each exposure, following the standard jitter procedure allowing for clean subtraction of the blank sky emission in IR. On several occasions, we observed 3 photometric standard stars from the

⁷ See <http://cdsweb.u-strasbg.fr/denis.html>

⁸ See <http://www.ipac.caltech.edu/2mass/releases/second/doc/>

⁹ See <http://www.astro.wisc.edu/sirtf/>

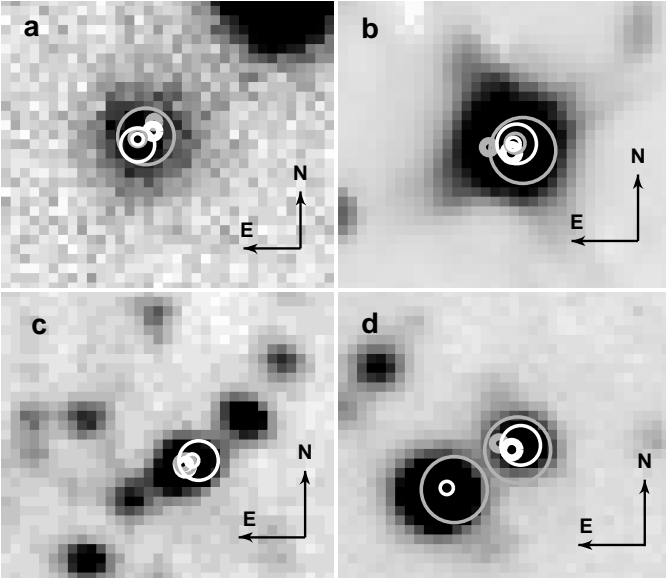


FIG. 5.— NTT images for (a) IGR J16195–4945 (I -band), (b) IGR J16207–5129 (K_s -band), (c) IGR J16167–4957 (K_s -band), and (d) IGR J17195–4100 (K_s -band). The lengths of the N and E arrows are $2''$. From smallest to largest, the error circles are: 2MASS (thin white, $0''.2$ radius error circle), USNO-B1.0 (thick grey, $0''.2$), USNO-A2.0 (thick white, $0''.25$), GLIMPSE (thin grey, $0''.3$), *Chandra* (thin white, $0''.6$), DENIS (thin grey, $1''$).

faint IR standard star catalog of Persson et al. (1998): sj9157, sj9172, and sj9181. We used the Image Reduction and Analysis Facility (IRAF) suite to perform data reduction, carrying out standard procedures of optical and NIR image reduction, including flat-fielding and NIR sky subtraction. We carried out aperture photometry, and we then transformed instrumental magnitudes into apparent magnitudes. The targets were close to the zenith during the observations.

Table 5 provides the results of our search of the catalogs, and also the results of our NTT observations. For each of the 5 catalogs, we list the closest source to the *Chandra* position and the measured magnitudes. In Figure 5, we show an I -band NTT image for IGR J16195–4945, and K_s -band images for the other three sources. The *Chandra* positions and the positions obtained from the catalogs are plotted on these images.

For IGR J16195–4945, the *Chandra* position lies on an apparently stellar IR source (based on an inspection of the 2MASS images) with a magnitude of $J = 13.57 \pm 0.03$. The 2MASS and GLIMPSE positions lie inside the *Chandra* error circle, indicating a good association between the X-ray and IR sources (see Figure 5a). However, the USNO-A2.0 position lies on the edge of the *Chandra* error circle, and the USNO-B1.0 position lies slightly outside. This may indicate the presence of a second optical source blended with the counterpart. Due to the faintness of the source (or sources) it is not clear from the NTT I -band image whether there are two blended sources or not. However, we present analysis of the spectral energy distributions (SEDs) below, and the IGR J16195–4945 SED (see Figure 6a) supports the possibility that there are two blended sources.

For IGR J16207–5129, the *Chandra* position lies on a bright IR source with $J = 10.44 \pm 0.02$. This source is present in all 5 catalogs, and all the positions are consistent with the *Chandra* source except for the USNO-B1.0 position, which lies just outside the *Chandra* error circle (see Figure 5b).

While this could indicate the presence of an interloper, the SED does not suggest any contamination by other sources (see Figure 6b).

For IGR J16167–4957, the *Chandra* position lies on a source with $J = 14.86 \pm 0.06$. The source appears in the GLIMPSE, 2MASS, and USNO catalogs, and all positions lie within the *Chandra* error circle (see Figure 5c). Although the 2MASS images suggest that the source is extended to the South-East, the NTT K_s -band image shows that there is actually a blend of at least 3 sources. The IGR J16167–4957 *Chandra* position is consistent with the brightest of the blended IR sources, but there is some suggestion in the NTT image that the brightest “source” may also be a blend.

For IGR J17195–4100, the *Chandra* position is near two sources that are clearly blended in the 2MASS images. The position of the 2MASS source is $2''.6$ away from the *Chandra* position, indicating that the bright IR source is not IGR J17195–4100. With I -band and IR coverage, both sources appear in the DENIS survey, and the optically-brighter, North-West source is the one that is consistent with the *Chandra* position. Our results confirm the association between IGR J17195–4100 and USNO-B1.0 0489–0511283.

7. SPECTRAL ENERGY DISTRIBUTIONS

Figure 6 shows the spectral energy distributions (SEDs) for the four sources. These include the optical and IR measurements given in Table 5, the spectrum in the *Chandra* bandpass, and *INTEGRAL* measurements. It should be noted that the optical and IR fluxes are not dereddened, and absorption is not removed from the *Chandra* spectra. The SED measurements are spread over a period of years, so discontinuities in the SED may be due to source variability. For the IR and optical parts of the SED, a check on variability is provided by the fact that we have multiple measurements for many of the photometric bands. A comparison shows that the IR fluxes are quite stable for IGR J16195–4945, IGR J16207–5129, and IGR J16167–4957. For IGR J16195–4945, the $1-\sigma$ error regions overlap for the J - and K_s -band measurements from DENIS and 2MASS. For IGR J16207–5129, the DENIS, 2MASS, and NTT J - and K_s -band measurements only range from 10.38–10.54 and 9.13–9.18, respectively. For IGR J16167–4957, the 2MASS and NTT measurements are consistent at the $1-\sigma$ level for J , H , and K_s . For IGR J16207–5129, the optical flux also appears to be rather stable, but for IGR J16195–4945 and IGR J16167–4957, the agreement between the various optical measurements is not as good (see Figure 6). For IGR J17195–4100, the agreement in the optical bands is relatively good, but this source has the sparsest optical/IR measurements.

For IGR J16195–4945, we simply show in Figure 6a the data and the best fit model for *Chandra*; however, for the other three sources, the spectrum is significantly distorted by pile-up, and we show the range of flux measurements based on the error ranges for the model parameters. For IGR J16207–5129, the flux range shown reflects the 90% confidence error range on Γ , which is 0.0–1.1. For IGR J16167–4957 and IGR J17195–4100, the Γ ranges are 0.7–1.6 and 0.8–1.4, respectively. The *INTEGRAL* 20–50 keV measurements and 50–250 keV upper limits are shown. As described in §5, the fits shown include a high energy cut off and a free normalization between *Chandra* and ISGRI. IGR J16207–5129 is the only source for which the normalization for ISGRI relative to *Chandra* is required to be less than 1.0, and this is apparent in Figure 6.

To characterize the shape of the optical and IR contin-

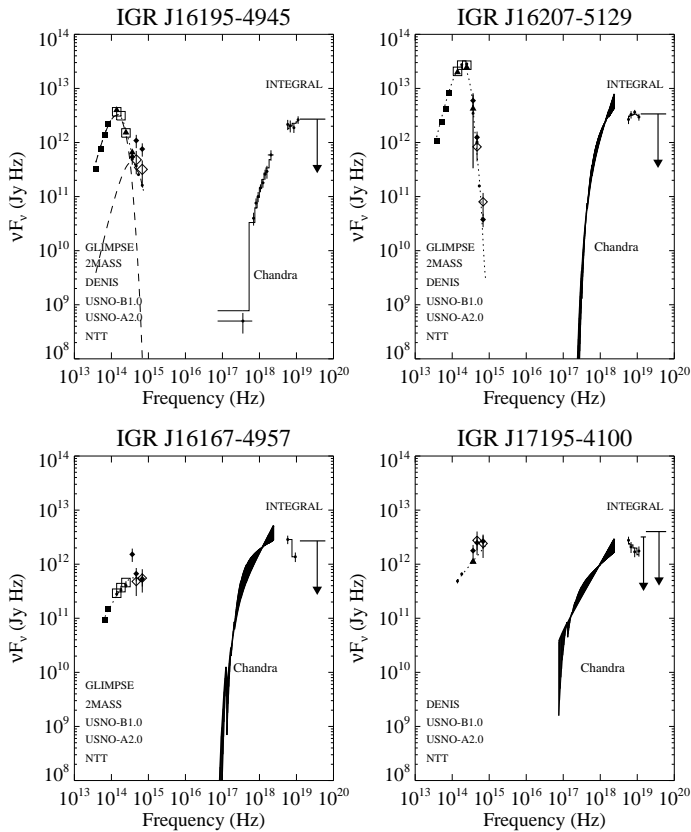


FIG. 6.— Spectral energy distributions (SEDs) for the four IGR sources. The IR and optical fluxes come from the measurements given in Table 5, and this part of the spectrum has been fitted with a blackbody model modified by the effects of extinction. The dotted line indicates the best fit (see text). *Chandra* and *INTEGRAL* measurements are also shown. For IGR J16207–5129, IGR J16167–4957, and IGR J17195–4100, our best estimate of the spectrum in the *Chandra* energy range is the model (solid line). For the optical/IR data, the different symbols are: GLIMPSE (filled squares), 2MASS (open squares), DENIS (filled triangles), USNO-B1.0 (filled diamonds), USNO-A2.0 (open diamonds), NTT (filled circles).

uum, we fitted each of the SEDs with four models: a single blackbody, a single power-law, the sum of 2 blackbodies, and a blackbody plus a power-law. Presumably, blackbody components could be indicative of thermal components from a star, but we consider the power-law to be a phenomenological component. The models also account for interstellar extinction using the analytical approximation of Cardelli, Clayton & Mathis (1989). This adds a single free parameter, A_V , to the single component models, while, for the two-component models, we allow the components to have different extinctions. We used χ^2 -minimization when fitting the SEDs, and, for IGR J16195–4945 and IGR J16207–5129, all of the models resulted in formally very poor fits with the best models leading to $\chi^2/\nu = 128/14$ and $\chi^2/\nu = 684/16$ for the two sources, respectively. Such poor fits may indicate inadequacies of our models, but they are also at least in part due to systematic errors, which may be related to the variability discussed above or possibly due to, e.g., uncertainties in magnitude/flux conversion. While it is clear that systematic errors must be included for these 2 sources, it is not clear which data points are the most suspect. Thus, we included systematic errors by simply multiplying the existing errors on all of the optical and IR data points by a constant factor. We adjusted the constant factor until we achieved a reduced- χ^2

of 1.0 for at least one of the models. For IGR J16195–4945 and IGR J16207–5129, the constant factors are 2.2 and 6.5, respectively. For the other 2 sources, IGR J16167–4957 and IGR J17195–4100, we did not need to include any systematic errors. The SED fit results are presented in Table 6, and here, we describe the results for each source in turn.

For IGR J16195–4945, neither of the single component models provide an acceptable fit to the optical/IR SED, and a two-component model is required at high significance. The two blackbody and blackbody plus power-law models provide acceptable fits, and both imply that the IR flux is dominated by a high temperature star (>9400 K) with high extinction ($A_V \sim 18$). Also, both models imply that the component that dominates the optical flux has a significantly lower extinction ($A_V < 7.1$). This SED and the shift between the optical and IR source positions reported in §6 provide evidence that the optical component comes from an interloping star, while the IR component likely comes from IGR J16195–4945.

Our highest quality optical/IR SED is the one for IGR J16207–5129. For this SED, two-component models do not provide any improvement over the single component models, and the blackbody and power-law models provide fits of roughly the same quality. The power-law index is $\alpha = -2.29^{+0.24}_{-0.28}$, which is nearly consistent with the value of $\alpha = -2$ expected for a blackbody. The fits strongly suggest that the spectrum is thermal as would be expected for stellar emission. From the blackbody fit, the value obtained for the extinction, $A_V = 10.8^{+0.3}_{-0.8}$ is very close to the value of $A_V = 9.5$ obtained by converting the Galactic column density of $N_H = 1.7 \times 10^{22}$ cm^{-2} to optical extinction using the Predehl & Schmitt (1995) relationship.

A blackbody model does not provide a good fit to the IGR J16167–4957 and IGR J17195–4100 SEDs with values of χ^2/ν of 54/10 and 26/6, respectively. However, both SEDs are adequately described by a power-law model with indices of $\alpha = -0.36^{+0.17}_{-0.18}$ and $\alpha = 0.17^{+0.12}_{-0.47}$, respectively. The power-law fits for both sources imply low extinction, which is consistent with the values of N_H measured via fits to the X-ray spectrum. Although we fitted the SEDs for these two sources with the two component models, the improvements in χ^2 do not justify the addition of another component, and the parameters for the two-component fits are very poorly constrained.

8. DISCUSSION

In the following, we discuss the detailed constraints on the nature of each source, considering the information we have obtained from *Chandra*, *INTEGRAL*, and the optical/IR SEDs.

8.1. IGR J16195–4945

Of our 4 sources, IGR J16195–4945 is the most similar to the class of obscured IGR sources. At $N_H = (7^{+5}_{-3}) \times 10^{22}$ cm^{-2} , the X-ray measured column density is higher than the Galactic value of 2.2×10^{22} cm^{-2} , suggesting the possibility that the X-ray source is intrinsically absorbed. Due to the possibility of intrinsic absorption, we cannot use the X-ray-measured N_H to constrain the distance to the source; however, because the optical and IR emission from the system is likely to predominantly come from regions that are not as affected by intrinsic absorption, such as the companion star, we expect that the optical extinction is dominated by interstellar material. Thus, the fact that $A_V = 17.5^{+0.8}_{-2.3}$ for the extinction on the blackbody component is as large or larger than the value obtained by converting the Galactic N_H to optical extinction ($A_V = 12.3$),

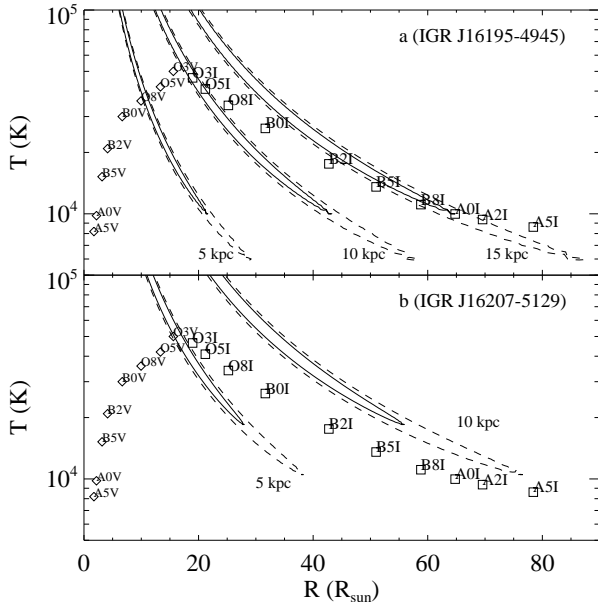


FIG. 7.— Error contours for IGR J16195–4945 (a) and IGR J16207–5129 (b) for the blackbody parameters in the optical/IR SEDs. Contours are shown for the stellar radius (R) and temperature (T), assuming various distances. The solid contours are 68% confidence ($\Delta\chi^2 = 2.3$), and the dashed contours are 90% confidence ($\Delta\chi^2 = 4.6$). Radii and temperatures for various spectral types from de Jager & Nieuwenhuijzen (1987) are overplotted, allowing us to constrain the likely spectral types of the companions in these systems.

is likely to indicate that we are looking at the source through much of the Galaxy. The distance to the Norma-Cygnus arm along this line of sight is ~ 5 kpc (Russeil 2003), and, although we cannot formally constrain the distance to the source, we assume a fiducial value of 5 kpc. From the unabsorbed fluxes reported in Table 3 and 4, the implied X-ray luminosities are $1.4 \times 10^{34} (d/5 \text{ kpc})^2$ (0.3–10 keV) ergs s^{-1} and $5.8 \times 10^{34} (d/5 \text{ kpc})^2 \text{ergs s}^{-1}$ (20–50 keV).

The IR portion of the SED is consistent with a single-temperature blackbody, suggesting that it is more likely that the IR emission comes from a stellar companion than from, e.g., an accretion disk. The lack of variability in the IR emission discussed in §7 also provides evidence that the emission comes from a star. The fit to the SED gives a lower limit on the blackbody temperature of $T > 9400$ K, and this indicates a spectral type earlier than A1–A2 regardless of whether the star is a main sequence star or a supergiant (de Jager & Nieuwenhuijzen 1987; Cox 2000). The question of whether the companion is a main sequence star or a supergiant depends sensitively on the distance to the source. In the fit to the SED, the parameters T and R/d have a significant level of degeneracy, and, in Figure 7a, we show 68% and 90% confidence error contours for T and R for assumed distances of 5 kpc, 10 kpc, and 15 kpc along with temperatures and radii for stars with various spectral types. If the distance is ~ 3 –9 kpc, the companion is a main sequence B or O-type star. If the distance is ~ 9 –15 kpc, a large range of supergiant A, B, and O-type spectral types are possible.

8.2. IGR J16207–5129

Like IGR J16195–4945, the IGR J16207–5129 N_{H} is somewhat (about a factor of 2) higher than the Galactic value, allowing for, but not requiring, some intrinsic absorption. From

the optical/IR SED, $A_V = 10.8^{+0.3}_{-0.8}$, and this value suggests a relatively large distance for this source. Thus, it is reasonable to take 5 kpc, the distance to the Norma-Cygnus arm along the line of sight, as a fiducial distance. The implied 0.3–10 keV luminosity is $1.3 \times 10^{35} (d/5 \text{ kpc})^2 \text{ergs s}^{-1}$, about an order of magnitude higher than IGR J16195–4945, and the 20–50 keV luminosity is $8.3 \times 10^{34} (d/5 \text{ kpc})^2 \text{ergs s}^{-1}$.

In this case, the optical/IR SED consists of a single-temperature blackbody, and it is very likely that this emission comes from the stellar companion. The lower limit on the stellar temperature is $> 18,000$ K, indicating that this system harbors a very hot, and likely massive, star. Figure 7 shows the error contours for the parameters T and R assuming distances of 5 and 10 kpc. At ~ 3 –5 kpc, the companion is a main sequence B or O-type star. At ~ 5 –9 kpc, various supergiant types are possible. At 10 kpc, the range of possible temperatures and radii are not consistent with any known spectral type, indicating that this system is closer than 10 kpc.

8.3. IGR J16167–4957

Although this source is close to the Galactic plane at $b = +0.50^\circ$ and is within 0.5° of IGR J16195–4945 and 1.7° of IGR J16207–5129, its X-ray spectrum indicates a column density of $N_{\text{H}} = (5^{+3}_{-2}) \times 10^{21} \text{cm}^{-2}$, which is an order of magnitude lower than the value for IGR J16195–4945 and is also lower than the Galactic column density of $2.2 \times 10^{22} \text{cm}^{-2}$ along this line of sight. The measured N_{H} corresponds to an extinction of $A_V = 2.8^{+1.7}_{-1.1}$, and, although the optical/IR SED is fit with a phenomenological power-law model, the implied extinction is even lower, $A_V = 1.3^{+0.6}_{-0.5}$. While the inhomogeneous distribution of gas and dust in the Galaxy make it difficult to use extinction measurements to determine source distances in any rigorous way, here, we make an estimate using the values from the Diplais & Savage (1994) study, which includes UV extinction measurements of nearly 400 early-type stars through various lines of sight through the Galaxy and with distances as large as 10 kpc. In that study, the average extinction per kpc is $A_V/d = 0.45$ magnitudes/kpc. For IGR J16167–4957, the extinction inferred from the X-ray spectrum allows the distance to be anywhere from 2 to 10 kpc, but the optical/IR extinction implies a distance of $2.9^{+1.3}_{-1.1}$ kpc. This estimate is marginally consistent with the source being in the Norma-Cygnus arm at ~ 5 kpc, but the line of sight also crosses the Scutum-Crux arm at ~ 3 kpc. Given the lower extinction for this source compared to IGR J16195–4945 and IGR J16207–5129, which are likely in the Norma-Cygnus arm, we take 3 kpc as a fiducial distance for IGR J16167–4957, and the X-ray luminosities are $4.7 \times 10^{34} (d/3 \text{ kpc})^2 \text{ergs s}^{-1}$ (0.3–10 keV) and $1.7 \times 10^{34} (d/3 \text{ kpc})^2 \text{ergs s}^{-1}$ (20–50 keV).

The interpretation for the shape of the optical/IR SED is not immediately clear, but the fact that it is not consistent with a single temperature blackbody suggests that the emission is not simply from a companion star. The power-law index of $-0.36^{+0.17}_{-0.18}$ is considerably flatter than a blackbody, and this could indicate a multi-temperature blackbody as might be expected from an accretion disk. Regardless of the dominant contributor to the optical/IR emission, we can take the measured magnitudes as an upper limit on the contribution from a putative optical companion. If we assume a distance and an extinction at the upper ends of the derived ranges, 4.2 kpc and $A_V = 2.8$, respectively, and interpolate between the measured B and R magnitudes to infer a V -band magnitude of 16.5, the limit on the absolute magnitude is $M_V > 0.6$. Unless

the distance is very much larger than 4.2 kpc, this rules out a supergiant companion, and the companion's spectral type is later than A0V. Thus, IGR J16167–4957 is not an HMXB.

8.4. IGR J17195–4100

At $l = 346.98^\circ$ and $b = -2.14^\circ$, this source is $\sim 14^\circ$ from the other 3 sources, and is slightly off the Galactic plane. The measured upper limit on the column density of $N_{\text{H}} < 2 \times 10^{21} \text{ cm}^{-2}$ is considerably lower than the Galactic value of $7.7 \times 10^{21} \text{ cm}^{-2}$, indicating that the distance to the source may be relatively low. The N_{H} from the X-ray spectrum implies $A_V < 1.18$, and the optical/IR SED gives an upper limit of $A_V < 0.96$. Using the average value of A_V/d from DiPlas & Savage (1994) indicates a distance upper limit in the range $d < 2.1$ – 2.6 kpc. The upper limit on the distance of 2.6 kpc implies upper limits on the X-ray luminosities of $< 2.0 \times 10^{34} \text{ ergs s}^{-1}$ (0.3–10 keV) and $< 1.6 \times 10^{34} \text{ ergs s}^{-1}$ (20–50 keV).

Like IGR J16167–4957, the physical interpretation for the power-law shape of the optical/IR SED is not clear. We can take the optical/IR magnitudes observed as upper limits on the contribution from a companion star. Interpolating between the B and R -bands, we estimate that $V = 14.8$. This, along with the highest upper limits we measure for the extinction, $A_V < 1.18$, and distance, $d < 2.6$ kpc, imply an upper limit on the absolute magnitude of $M_V < 1.5$. This rules out a supergiant companion or an OB main sequence star. The earliest spectral type possible is $\sim A3V$.

9. SUMMARY OF THE NATURE OF THE 4 IGR SOURCES

Table 7 contains a summary of the results described in §8, including constraints on the source distance, X-ray luminosities, and possible spectral types. Our basic conclusion is that IGR J16195–4945 and IGR J16207–5129 are very likely HMXBs and are at distances consistent with the Norma-Cygnus arm (although the distances are not well enough constrained to say definitively that they are in this spiral arm), while the other two IGR sources (IGR J16167–4957 and IGR J17195–4100) are nearer and are not HMXBs. Assuming distances of 5 kpc for the 2 HMXBs, the 0.3–10 keV luminosities are $10^{34-35} \text{ ergs s}^{-1}$, which is, not surprisingly, significantly lower than the brightest HMXB pulsars (e.g., Vela X-1, Cen X-3), but the luminosities are not atypical when considering the full range of HMXB pulsar luminosities.

Of the 4 IGR sources, only IGR J16195–4945 has a column density that is consistent with the source having significant intrinsic absorption. While IGR J16207–5129 could conceivably also have some level of intrinsic absorption, comparing its column density to the Galactic value suggests that the intrinsic N_{H} is not more than $\sim 1 \times 10^{22} \text{ cm}^{-2}$ while many IGR sources have $N_{\text{H}} \sim 10^{23-24} \text{ cm}^{-2}$. From the perspective of IGR sources and HMXB evolution (Dean et al. 2005), the very high column density IGR sources may be in an evolutionary stage during which the neutron star is spiraling to-

ward its companion, becoming embedded in the wind from the high-mass companion. In this picture, we may be seeing IGR J16207–5129 early in this evolutionary phase so that the neutron star is still in a low density portion of the wind. Source-to-source differences in N_{H} could also be indicative of variations in the strength of the stellar wind over time.

After submission of this work, two other reports provided further information about the HMXBs. Using *INTEGRAL*, Sguera et al. (2006) found a 1.5 hour X-ray outburst from IGR J16195–4945, indicating that this source may belong to the class of supergiant fast X-ray transients. Also, for IGR J16207–5129, Masetti et al. (2006a) report on optical spectra of USNO-A2.0 0375-27093111 (i.e., the same star that we have determined to be the counterpart), and find that the spectrum includes $H\alpha$ in emission and is consistent with that of an HMXB.

Masetti et al. (2006a) also report on the optical spectra of the stars that we have (independently) determined to be the optical counterparts of IGR J17195–4100 and IGR J16167–4957. These stars show Hydrogen Balmer series emission lines as well as HeI and HeII emission lines. While this indicates that they are either Cataclysmic Variables (CVs) or LMXBs, the hard X-ray spectra would be very unusual for LMXBs (e.g., Muno et al. 2004). A CV interpretation is more likely, and Masetti et al. (2006a) also come to this conclusion.

JAT acknowledges partial support from *Chandra* award number GO5-6037X issued by the *Chandra X-Ray Observatory Center*, which is operated by the Smithsonian Astrophysical Observatory for and on behalf of the National Aeronautics and Space Administration (NASA), under contract NAS8-03060. JAT acknowledges partial support from a NASA *INTEGRAL* Guest Observer grant NNG05GC49G. LF acknowledges partial funding from the Italian Space Agency (ASI) under contract I/R/046/04 and from MIUR under contract COFIN 2004-023189. We thank the referee for helpful comments that improved this manuscript. This work is based, in part on ESO observations through program #073.D-0339. We thank the referee for helpful comments that improved this manuscript. This publication makes use of data products from the Two Micron All Sky Survey, which is a joint project of the University of Massachusetts and the Infrared Processing and Analysis Center/California Institute of Technology, funded by NASA and the National Science Foundation. This research has made use of the USNOFS Image and Catalogue Archive operated by the United States Naval Observatory, Flagstaff Station as well as the SIMBAD database, operated at CDS, Strasbourg, France. We have also used data from *Spitzer's* Galactic Legacy Infrared Mid-Plane Survey Extraordinaire (GLIMPSE) as well as the Deep Near Infrared Survey of the Southern Sky (DENIS).

REFERENCES

- Beckmann, V., et al., 2005, *ApJ*, 631, 506
 Bird, A. J., et al., 2006, *ApJ*, 636, 765
 Bird, A. J., et al., 2004, *ApJ*, 607, L33
 Bodaghee, A., Walter, R., Zurita Heras, J. A., Bird, A. J., Courvoisier, T. J.-L., Malizia, A., Terrier, R., & Ubertini, P., 2006, *A&A*, 447, 1027
 Cardelli, J. A., Clayton, G. C., & Mathis, J. S., 1989, *ApJ*, 345, 245
 Cash, W., 1979, *ApJ*, 228, 939
 Coburn, W., Heindl, W. A., Rothschild, R. E., Gruber, D. E., Kreykenbohm, I., Wilms, J., Kretschmar, P., & Staubert, R., 2002, *ApJ*, 580, 394
 Combi, J. A., Ribó, M., Mirabel, I. F., & Sugizaki, M., 2004, *A&A*, 422, 1031
 Cox, A. N., 2000, *Allen's astrophysical quantities*, 4th ed. Publisher: New York: AIP Press; Springer, 2000. Edited by Arthur N. Cox.)
 Davis, J. E., 2001, *ApJ*, 562, 575
 de Jager, C., & Nieuwenhuijzen, H., 1987, *A&A*, 177, 217
 Dean, A. J., et al., 2005, *A&A*, 443, 485
 Dickey, J. M., & Lockman, F. J., 1990, *ARA&A*, 28, 215
 DiPlas, A., & Savage, B. D., 1994, *ApJ*, 427, 274
 Filliatre, P., & Chaty, S., 2004, *ApJ*, 616, 469
 Freeman, P. E., Kashyap, V., Rosner, R., & Lamb, D. Q., 2002, *ApJS*, 138, 185

TABLE 1
Chandra OBSERVATIONS

Obs ID	Target	l^a	b^b	Start Time	Exposure Time (s)
5471	IGR J16195–4945	333.56	+0.34	2005 April 29, UT 17:25	4,752
5472	IGR J16207–5129	332.46	–1.05	2005 June 25, UT 03:17	5,109
5473	IGR J16167–4957	333.06	+0.50	2005 June 13, UT 19:14	4,979
5474	IGR J17195–4100	346.98	–2.14	2005 July 25, UT 12:57	4,701

^aGalactic longitude in degrees.

^bGalactic latitude in degrees.

TABLE 2
Chandra COUNT RATES AND POSITIONS

IGR Name	CXOU Name	ACIS Rate ^a	R.A. ^b	Decl. ^c	X-Ray Identification
J16195–4945	J161932.2–494430	0.039	16 ^h 19 ^m 32 ^s .20	–49°44′30″.7	AX J161929–4945(?)
J16207–5129	J162046.2–513006	0.13	16 ^h 20 ^m 46 ^s .26	–51°30′06″.0	–
J16167–4957	J161637.7–495844	0.18	16 ^h 16 ^m 37 ^s .74	–49°58′44″.5	1RXS J161637.2–495847
J17195–4100	J171935.8–410053	0.15	17 ^h 19 ^m 35 ^s .88	–41°00′53″.6	1RXS J171935.6–410054

^aCount rate detected by the ACIS-I instrument in the 0.3–10 keV bandpass.

^bRight Ascension (equinox J2000). The radius of the error circle is 0″.6.

^cDeclination (equinox J2000). The radius of the error circle is 0″.6.

TABLE 3
Chandra SPECTRAL RESULTS

IGR Name	N_{H}^a ($\times 10^{22}$ cm ^{–2})	Γ	Flux ^b	α^c	Fit Statistic ^d	Galactic N_{H}^e ($\times 10^{22}$ cm ^{–2})
J16195–4945	7 ⁺⁵ _{–3}	0.5 ^{+0.9} _{–0.7}	4.6 ^{+2.1} _{–0.8}	–	453	2.2
J16207–5129	3.7 ^{+1.4} _{–1.2}	0.5 ^{+0.6} _{–0.5}	42 ⁺⁹ _{–7}	0.43 ^{+0.10} _{–0.09}	667	1.7
J16167–4957	0.5 ^{+0.3} _{–0.2}	1.1 ^{+0.5} _{–0.4}	44 ⁺¹¹ _{–10}	0.62 ^{+0.06} _{–0.07}	701	2.2
J17195–4100	0.08 ^{+0.13} _{–0.08}	1.1 ± 0.3	25 ⁺⁹ _{–4}	0.64 ^{+0.09} _{–0.10}	743	0.77

^aErrors in this table are at the 90% confidence level ($\Delta C = 2.7$).

^bUnabsorbed 0.3–10 keV flux in units of 10^{-12} erg cm^{–2} s^{–1}.

^cThe grade migration parameter in the pile-up model (Davis 2001). The probability that n events will be piled together but will still be retained after data filtering is α^{n-1} .

^dThe Cash statistic for the best fit model. In each case, the spectra include 663 energy bins.

^eThe column density through the Galaxy from Dickey & Lockman (1990).

Garmire, G. P., Bautz, M. W., Ford, P. G., Nousek, J. A., & Ricker, G. R., 2003, in *X-Ray and Gamma-Ray Telescopes and Instruments for Astronomy*. Edited by Joachim E. Truemper, Harvey D. Tananbaum. Proceedings of the SPIE, 4851, 28

Landolt, A. U., 1992, *AJ*, 104, 340

Lebrun, F., et al., 2003, *A&A*, 411, L141

Lutovinov, A., Revnivtsev, M., Gilfanov, M., Shtykovskiy, P., Molkov, S., & Sunyaev, R., 2005a, *A&A*, 444, 821

Lutovinov, A., Rodriguez, J., Revnivtsev, M., & Shtykovskiy, P., 2005b, *A&A*, 433, L41

Masetti, N., Morelli, L., Palazzi, E., Stephen, J., Bazzano, A., Dean, A. J., Walter, R., & Minniti, D., 2006a, *The Astronomer’s Telegram*, 783, 1

Masetti, N., et al., 2006b, *A&A*, 449, 1139

Matt, G., & Guainazzi, M., 2003, *MNRAS*, 341, L13

Muno, M. P., et al., 2004, *ApJ*, 613, 1179

Negueruela, I., Smith, D. M., Harrison, T. E., & Torrejón, J. M., 2006, *ApJ*, 638, 982

Persson, S. E., Murphy, D. C., Krzeminski, W., Roth, M., & Rieke, M. J., 1998, *AJ*, 116, 2475

Predehl, P., & Schmitt, J. H. M. M., 1995, *A&A*, 293, 889

Revnivtsev, M. G., 2003, *Astronomy Letters*, 29, 644

Rodriguez, J., Tomsick, J. A., Foschini, L., Walter, R., Goldwurm, A., Corbel, S., & Kaaret, P., 2003, *A&A*, 407, L41

Russeil, D., 2003, *A&A*, 397, 133

Sguera, V., et al., 2006, *astro-ph/0603756*

Sidoli, L., Vercellone, S., Mereghetti, S., & Tavani, M., 2005, *A&A*, 429, L47

Smith, D. M., Heindl, W. A., Markwardt, C. B., Swank, J. H., Negueruela, I., Harrison, T. E., & Huss, L., 2006, *ApJ*, 638, 974

Stephen, J. B., et al., 2005, *A&A*, 432, L49

Sugizaki, M., Mitsuda, K., Kaneda, H., Matsuzaki, K., Yamauchi, S., & Koyama, K., 2001, *ApJS*, 134, 77

Tomsick, J. A., Corbel, S., Goldwurm, A., & Kaaret, P., 2005, *ApJ*, 630, 413

Tomsick, J. A., Lingenfelter, R., Corbel, S., Goldwurm, A., & Kaaret, P., 2004, in *ESA SP-552: 5th INTEGRAL Workshop on the INTEGRAL Universe*, 413

Ubertini, P., et al., 2003, *A&A*, 411, L131

Ueda, Y., et al., 1999, *ApJ*, 518, 656

Walter, R., et al., 2003, *A&A*, 411, L427

Weisskopf, M. C., Brinkman, B., Canizares, C., Garmire, G., Murray, S., & Van Speybroeck, L. P., 2002, *PASP*, 114, 1

Winkler, C., et al., 2003, *A&A*, 411, L1

TABLE 4
INTEGRAL SPECTRAL RESULTS

IGR Name	Exposure Time (ks)	Count Rate ^a	Γ	Flux ^b	χ^2/ν
J16195–4945	167	0.24 ± 0.03	1.7 ± 0.8	19 ± 3	1.3/2
J16207–5129	165	0.35 ± 0.03	1.9 ± 0.5	28 ± 3	2.5/2
J16167–4957	167	0.18 ± 0.03	$4.3_{-1.4}^{+1.6}$	16_{-4}^{+3}	0/0
J17195–4100	495	0.23 ± 0.02	2.8 ± 0.8	19 ± 3	1.1/2

^a20–50 keV ISGRI count rate.

^b20–50 keV flux in units of 10^{-12} erg cm⁻² s⁻¹.

TABLE 5
OPTICAL AND IR MAGNITUDES OR FLUXES

	IGR J16195–4945	IGR J16207–5129	IGR J16167–4957	IGR J17195–4100
USNO-B1.0				
Name ^a	0402-0529810	0384-0560875	0400-0527262	0489-0511283
Separation ^b	1''.03	0''.81	0''.53	0''.70
<i>B</i>	16.5 ± 0.3	19.7 ± 0.3	16.8 ± 0.3	15.1 ± 0.3
<i>R</i>	15.3 ± 0.3	15.2 ± 0.3	15.8 ± 0.3	14.4 ± 0.3
<i>I</i>	15.6 ± 0.3	13.0 ± 0.3	14.5 ± 0.3	14.3 ± 0.3
USNO-A2.0				
Name ^a	0375-27014824	0375-27093111	0375-26829054	0450-27095307
Separation ^b	0''.72	0''.31	0''.45	0''.31
<i>B</i>	17.4 ± 0.5	18.9 ± 0.5	16.8 ± 0.5	15.2 ± 0.5
<i>R</i>	16.2 ± 0.5	15.6 ± 0.5	16.2 ± 0.5	14.3 ± 0.5
DENIS				
Name ^a	J161932.1–494430	J162046.2–513006	—	J171935.8–410053
Separation ^b	0''.42	0''.29	—	0''.10
<i>I</i>	15.38 ± 0.05	13.4 ± 1.0	—	14.81 ± 0.04
<i>J</i>	13.55 ± 0.08	10.54 ± 0.05	—	—
<i>K_s</i>	10.92 ± 0.06	9.17 ± 0.06	—	—
2MASS				
Name ^a	J16193220–4944305	J16204627–5130060	J16163776–4958445	J17193608–4100548
Separation ^b	0''.14	0''.11	0''.26	2''.6
<i>J</i>	13.57 ± 0.03	10.44 ± 0.02	14.86 ± 0.06	— ^c
<i>H</i>	11.96 ± 0.03	9.62 ± 0.02	14.28 ± 0.09	— ^c
<i>K_s</i>	11.00 ± 0.02	9.13 ± 0.02	13.76 ± 0.10	— ^c
GLIMPSE				
Name ^a	G333.5571+00.3390	G332.4590–01.0501	G333.0560+00.4962	—
Separation ^b	0''.21	0''.07	0''.34	—
3.6 μ m	26.5 ± 1.1 mJy	100 ± 3 mJy	1.79 ± 0.16 mJy	—
4.5 μ m	20.3 ± 1.1 mJy	61 ± 3 mJy	1.40 ± 0.16 mJy	—
5.8 μ m	14.3 ± 1.0 mJy	46 ± 2 mJy	—	—
8.0 μ m	8.5 ± 0.5 mJy	28.4 ± 0.9 mJy	—	—
New Technology Telescope				
<i>B</i>	18.14 ± 0.06	19.8 ± 0.1	—	—
<i>V</i>	17.22 ± 0.05	17.74 ± 0.06	—	—
<i>R</i>	16.42 ± 0.05	15.38 ± 0.03	—	—
<i>I</i>	15.54 ± 0.03	13.58 ± 0.02	—	—
<i>J</i>	—	10.38 ± 0.02	15.0 ± 0.1	14.1 ± 0.1
<i>H</i>	—	9.60 ± 0.02	14.4 ± 0.1	13.65 ± 0.07
<i>K_s</i>	—	9.18 ± 0.04	13.8 ± 0.1	13.2 ± 0.1

^aName of the nearest star in the catalog.

^bSeparation between the *Chandra* position and the nearest star in the catalog.

^cThis 2MASS source is too far from the *Chandra* position to be associated.

TABLE 6
IR/OPTICAL SED FITS

	IGR J16195–4945	IGR J16207–5129	IGR J16167–4957	IGR J17195–4100
Blackbody				
A_V	<0.16	$10.8^{+0.3}_{-0.8}$	<1.16	<2.84
T (K)	1944^{+39}_{-42}	>18000	2790^{+350}_{-70}	4100^{+5500}_{-200}
R/d (R_\odot /kpc) ^a	10.3 ± 0.6	<5.53	1.84 ± 0.21	$1.40^{+0.14}_{-0.62}$
χ^2/ν	269/16	23/19	54/10	26/6
Power-law				
A_V	7.1 ± 0.6	$11.6^{+0.8}_{-0.7}$	$1.3^{+0.6}_{-0.5}$	<0.96
α^b	-0.73 ± 0.13	$-2.29^{+0.24}_{-0.28}$	$-0.36^{+0.17}_{-0.18}$	$0.17^{+0.12}_{-0.47}$
N_{pl}^c	0.030 ± 0.003	0.27 ± 0.03	0.00191 ± 0.00015	0.0039 ± 0.0006
χ^2/ν	300/16	19/19	12/10	9/6
2 Blackbodies				
$A_{V,1}$	$17.5^{+0.8}_{-2.3}$	–	–	–
T_1 (K)	>9400	–	–	–
R_1/d (R_\odot /kpc)	<4.36	–	–	–
$A_{V,2}$	<4.89	–	–	–
T_2 (K)	>3800	–	–	–
R_2/d (R_\odot /kpc)	<1.13	–	–	–
χ^2/ν	12/14	23/17	8/7	7/3
Blackbody+Power-law				
$A_{V,bb}$	$17.5^{+0.8}_{-2.1}$	–	–	–
T (K)	>9500	–	–	–
R/d (R_\odot /kpc)	<4.25	–	–	–
$A_{V,pl}$	$4.3^{+2.8}_{-1.1}$	–	–	–
α^a	$-1.7^{+1.0}_{-2.9}$	–	–	–
N_{pl}^b	$0.0015^{+0.0020}_{-0.0013}$	–	–	–
χ^2/ν	12/14	18/17	8/7	5/3

^a R/d is the ratio of the radius of the spherical blackbody (in R_\odot) to the distance to the source (in kpc).

^bThe power-law index, defined according to $F_\nu \propto \nu^{-\alpha}$.

^cThe power-law normalization, corresponding to the flux in Jy at a reference frequency of 10^{14} Hz.

TABLE 7
SUMMARY OF RESULTS

IGR Name	d (kpc)	d_{fiducial} (kpc)	L (0.3–10 keV) ^a	L (20–50 keV) ^b	Spectral Type
J16195–4945	~3–15	5 (Norma-Cygnus?)	1.4×10^{34}	5.8×10^{34}	OBV or supergiant
J16207–5129	~3–10	5 (Norma-Cygnus?)	1.3×10^{35}	8.3×10^{34}	OBV or supergiant
J16167–4957	1.8–4.2	3 (Scutum-Crux?)	4.7×10^{34}	1.7×10^{34}	later than A0V
J17195–4100	<2.6	<2.6	$<2.0 \times 10^{34}$	$<1.6 \times 10^{34}$	later than A3V

^aThe X-ray luminosity in ergs s^{-1} measured by *Chandra* at the fiducial distance.

^bThe X-ray luminosity in ergs s^{-1} measured by *INTEGRAL* at the fiducial distance.